Int J Adv Manuf Technol (2016) 86:671–679
DOI 10.1007/s00170-015-8157-0

ORIGINAL ARTICLE

Experimental study on the process of adiabatic shear fracture in isolated segment formation in high-speed machining of hardened steel

Liyao Gu[1,2] · **Minjie Wang**[2] · **Hui Chen**[1] · **Guozheng Kang**[1]

Received: 24 May 2015 / Accepted: 24 November 2015 / Published online: 23 December 2015

Abstract Adiabatic shear fracture in serrated chip leads to isolated segment formation in high-speed machining with the further increase of cutting speed. An energy model of adiabatic shear band is built and investigated through high-speed machining tests and chip morphology examination. A quick-stop device designed to obtain chip roots in high-speed turning is applied. The adiabatic shear fracture process on considering the induced mechanism is investigated and the multi-stage physical model of adiabatic shear fracture is proposed through chip root morphology examination. The results show that adiabatic shear fracture in high-speed machining is a periodic process from energy convergence to release. The shear band collapses and results in isolated segments formation when the energy convergence in band exceeds the saturation limit. There are possibilities of utilizing the occurrence of adiabatic shear fracture to reduce the increased rate of stress, temperature, and energy and optimize the machinability in the chip formation aspect in high-speed machining.

Keywords High-speed machining · Adiabatic shear fracture · Isolated segment · Fracture · Quick-stop device

✉ Liyao Gu
guliyao0922@163.com

✉ Minjie Wang
mjwang@dlut.edu.cn

✉ Hui Chen
xnrpt@163.com

[1] State key Laboratory of Traction Power & Institute of Materials Science and Engineering, Southwest Jiaotong University, Chengdu, China

[2] Key Laboratory of the Ministry of Education for Precision and Non-traditional Machining, School of Mechanical Engineering, Dalian University of Technology, Dalian, China

1 Introduction

High-speed machining technology has been playing a critically important role in lots of developing manufacturing industries until nowadays and heatedly concerned and discussed by researchers and engineers as an advanced technical issue. One of the principle differences between conventional machining and high-speed machining is the chip morphology produced. As to most workpiece materials, adiabatic shear inevitably occurs due to a large and fast deformation and heating in primary shear zone, resulting in serrated chip formation and fracture induced by the evolution of adiabatic shear band (ASB), which has become one of the main characteristics in high-speed machining with the increase of cutting speed. Most of the early studies of adiabatic shear in high-speed machining focused on the onset stage of adiabatic shear and found that the occurrence of adiabatic shear resulting in serrated chip formation is caused by the local softening effect exceeding the strain and strain rate hardening in localized shear zone [1–5]. However, adiabatic shear band always acts as a damage carrier, and its formation implies that adiabatic shear fracture (or adiabatic shear localization fracture, ASLF) will occur subsequently [6, 7]. This fracture in ASB undergoes crack propagation and tears up the serrated chip into small isolated segments has been observed in some machining experiments. Adiabatic shear fracture is an inevitable fracture phenomenon due to adiabatic shear evolution. This fracture phenomenon is beneficial to chip breaking due to discontinuous cutting or even completely separated serrated chip in automatic machining process, reducing the loading area of shear plane, thus impeding the increase of cutting force. Adversely, adiabatic shear fracture–induced high-frequency oscillation of cutting force can influence the precision and surface quality. Thus, adiabatic shear fracture needs deeper investigation for its complicated influence on high-speed machining process.

Hitherto, the occurrence of adiabatic shear fracture in the final stage of adiabatic shear evolution results in serrated chip fracture which has been observed in some high-speed machining experiments. Komanduri et al. [8] hold that the serrated chip fracture is caused by the heat concentration in primary shear zone. Gente et al. [9] conducted a quick-stop experiment to obtain titanium alloy chip roots by using light-gas gun; the formation of adiabatic shear band, and crack propagation process are analyzed. Barry et al. [10] observed shear band propagation and the fracture surface of titanium alloy chip roots obtained through a quick-stop experiment. Hua and Shivpuri [11] applied Cockrof–Latham ductile fracture criterion and FEM software to simulate crack propagation in primary shear zone of titanium alloy at various cutting speeds. Su and Liu [12] investigated the influence of material brittleness on serrated chip formation through an orthogonal cutting experiment with four steels under different cutting conditions and suggested that the serrated chip fracture results from brittleness enhancement. Wang et al. [13] observed that the fracture occurs in serrated chip of high strength steel due to adiabatic shear evolution. Then, Gu et al. [14, 15] found that the formation and fracture of adiabatic shear band in serrated chip had energy-related regularity. The mechanism of adiabatic shear fracture in serrated chip so far lacks of a thorough understanding, and thus, it still needs studies to push forward deeper cognitions.

The purpose in present study is to investigate the process of adiabatic shear fracture in high-speed machining experimentally. The energy model of adiabatic shear band is built and investigated through high-speed machining tests and chip morphology examination. A quick-stop device is designed and applied to obtain chip roots in high-speed turning. On the basis of chip root morphology examination, the physical model of adiabatic shear fracture is proposed and the induced mechanism is investigated.

2 Model

In order to analyze strain and energy in ASB during the occurrence of adiabatic shear fracture, it is necessary to make some microscopic observation samples of serrated chips, and the geometry parameters of serrated chip at negative rake angle is shown in Fig. 1 based on our previous work [15]. The average shear strain rate and shear strain in shear band should be expressed as

$$\begin{cases} \dot{\gamma} = \dfrac{v\cos\gamma_0}{S\cos(\phi-\gamma_0)} \\ \gamma = \dfrac{G_S a_c}{S\sin\phi} \end{cases} \tag{1}$$

where v is the cutting velocity, a_c is the cutting thickness, a_h and a_{ch} are the height of serrated tooth and the chip thickness,

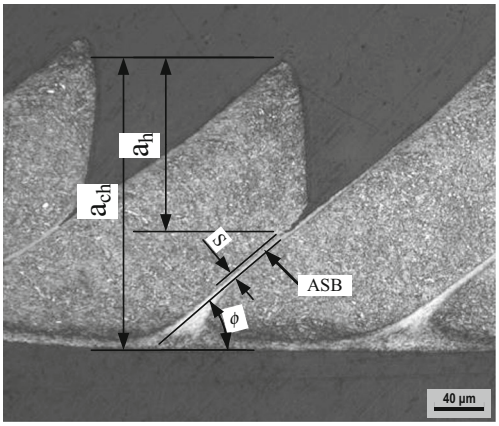

Fig. 1 Geometry parameters of serrated chip [15]

respectively, ϕ is the shear angle, γ_0 is the tool rake angle, S is the ASB width, and $G_S=a_h/a_{ch}$.

The stress state of compressive stress is σ and shear stress is τ in primary shear zone. The equivalent shear stress τ_e in plane strain condition is calculated as

$$\tau_e = \sqrt{\frac{\sigma^2}{3}+\tau^2} \tag{2}$$

where $\sigma=\tau\cot\phi$, and $\tau = \tau(\gamma,\dot{\gamma},\theta)$ is a constitutive relation. According to the work of Feng et al. [16], the modified Johnson–Cook conservative relation of the hardened steel is

$$\tau = \left[A + B\left(\frac{\gamma}{\sqrt{3}}\right)^n\right]\left[1 + C\ln\left(\frac{\dot{\gamma}}{\dot{\gamma}_0}\right)\right]\exp\left[-\left(\frac{\theta^*-m_1}{m_2}\right)^2\right] \tag{3}$$

where $\theta^*=(\theta-\theta_r)/(\theta_m-\theta_r)$. Assuming the shear banding process in the serrated chip formation is adiabatic, this assumption is reasonable when the cutting speed is large enough:

$$\theta = \frac{\beta}{\rho c}\int_0^{\gamma}\tau_e(\gamma,\dot{\gamma},\theta)\mathrm{d}\gamma + \theta_r \tag{4}$$

Accordingly, the energy in ASB can be calculated as

$$G_{ASB} = \int_0^{\gamma}\tau_e(\gamma,\dot{\gamma},\theta)d\gamma \tag{5}$$

3 Experimental

Hardened AISI 1045 steel is a typical structure metal being widely used in industry and selected as the workpiece. The chemical composition of this hardened steel is shown in Table 1. The thermo-physical parameters and the modified constitutive material parameters used in the calculation are listed in Tables 2 and 3. The hardened steel was machined into a cylindrical workpiece with a diameter of 300 mm and then

Table 1 Chemical composition of the hardened steel

C	Si	Mn	P	S	Cr	Ni
0.42~0.50	0.17~0.37	0.50~0.18	<0.04	<0.04	<0.25	<0.25

was quenched and tempered to a hardness of 45 HRC. The arrangement of machining setup is shown in Fig. 2. Machining tests were conducted on OKUMA Mill-Turn CNC by using straight edge of polycrystalline cubic boron Nitride (PCBN) insert cutting tool with the rake angle of −10° under dry cutting condition. A cylindrical workpiece tube with a thickness of 1.5 mm was machined and held by the lathe chuck, as shown in Fig. 2. It was to ensure that the plane strain condition could be prevailed during chip formation process. The tool feeding in the X-direction determines the cutting thickness. The cutting speed ranges from 100 to 1400 m/min; the feed is 0.2~0.3 mm/r. All tests were replicated at least two times.

In order to investigate the process of adiabatic shear fracture in serrated chip, it is essential to conduct quick-stop tests for obtaining chip roots under high-speed machining. A quick-stop device with auxiliary exempted plan through modifying Buda method [17] was designed for freezing the moment of shear band fracture and used in the condition of high-speed orthogonal machining (Fig. 3). Figure 3a illustrates the chip root arresting principle under different cutting conditions during high-speed orthogonal turning. In the device, a quick-stop workpiece with a hole and a kerf is designed to obtain chip root. Additionally, the inclined surface can protect the tool tip from breaking as it cuts into the workpiece. As shown in Fig. 3a, the dotted line is the tool tip trajectory related to the workpiece. The cutting speed is v, the cutting thickness is a_c, and the feed is f. The time of different tool cutting positions are t_0, t_1, and t_2, respectively. The fracture time of the chip root separating from the workpiece is t_f. The cutting thickness and the cutting force increase with tool path from time t_0 to t_1. The cutting thickness was unchanged after time t_1. As shown in Fig. 3a, the loading area between the tool tip and the hole reaches a minimum at the time t_f, the region of the tool engaged fractures due to the tensile force from the cutting force, and thus the chip root generates and separates from the workpiece. Additionally, the chip root can be quickly thrown away from the cutting setup due to centrifugal force resulting from the rotation of principal axes. The mass of the chip root which fractures from the workpiece body is about 0.1~0.2 g, and the cutting force at fracture is about the order of 700~1000 N. Thus, the arresting acceleration can be up to nearly 10^6~10^7 m/s^2 when the cutting speed is above 1000 m/min. As a result of such high accelerations, the amount of tool engaging during separating is very small compared to the cutting thickness. Based on the quick-stop principle described above, the arrangement of quick-stop experimental setup in high-speed turning is shown in Fig. 3b. The quick-stop workpieces are fixed on workpiece holder which is held in the lathe chuck through the mandrel. The cutting thickness is accurately controlled through setting the feed of the machine tool, and the new changed tool is adjusted every time through the tool detection. During the quick-stop tests, the cutting takes place on the straight edge of a triangular PCBN insert. The workpiece is clamped to a mandrel which is held in the lathe chuck. When the spindle is rotating at the required speed, the cutting tool feeds rapidly forward to a predefined position and held there firmly until the chip root is obtained. These quick-stop tests were performed at the onset conditions of adiabatic shear fracture which were obtained in the machining experiments. The tool rake angle was maintained constant at −10°, and only unworn tools were used.

Table 2 Thermo-physical parameters of the hardened steel

ρ (kg/m^3)	c (J/kg·K)	k (W/m·K)	T_m (°C)
7830	477	33.5	1520

Table 3 Constitutive parameters of modified Johnson–Cook model of the hardened steel

A (MPa)	B (MPa)	C	m_1	m_2	$\dot{\varepsilon}_0$	θ_r (°C)
691	244	0.064	−0.005989	0.4415	1	23

All the chips obtained in the cutting were set vertically into the mixture of epoxy resin and curing agent. Metallographic samples of the chip cross section are obtained through mounting, polishing, and etching in 4% nitric acid. The chip morphologies were observed by using a LEICA MeF-4 metallographic microscope. The isolated segment with fractured shear band was examined under a scanning electron microscope (SEM).

4 Results and discussions

4.1 Chip formation

The polished and etched mid-section micrographs of the chip specimens of the hardened steel at various cutting speeds up to

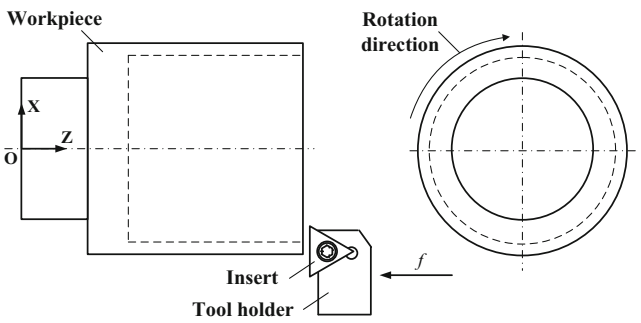

Fig. 2 General arrangement of high-speed machining setup

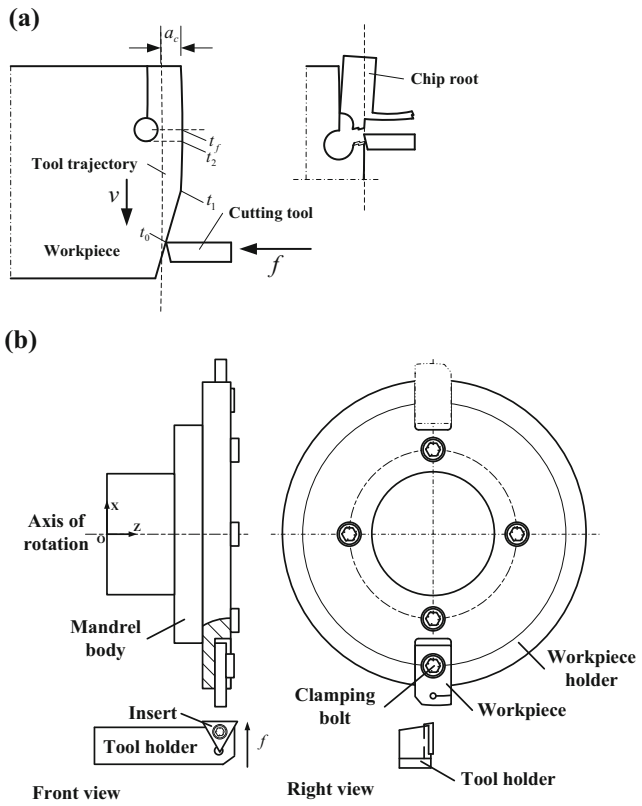

Fig. 3 Quick-stop principle (**a**) and its experimental setup (**b**) for obtaining chip root specimens

1300 m/min at the feed of 0.2 mm/r are shown in Fig. 4. Figure 4a shows a ribbon chip micrograph generated due to homogeneous plastic shear deformation at cutting speed of 100 m/min. At cutting speed of 500 m/min, the chip deformation becomes inhomogeneous due to adiabatic shear, and ribbon chip transforms into serrated chip with fully developed deformed bands which are not distinguished from the matrix after etching, and the grains are just elongated along the shear direction, as shown in Fig. 4b. Two deformation regions can be seen in the chip segments where one is deformed band with a moderate strain of about 5 and the other with a strain less than 1 according to Eq. (1). At cutting speed of 800 m/min, deformed bands transform into transformed bands which are distinguished from the matrix for the white color after etching due to the grain structure transformation under the extremely increased strain about 40. The microcracks have generated and begin to propagate along the transformed bands, as shown in Fig. 4c. With a further increase of cutting speed up to 1000 m/min, the serrated chips become discontinuously short with increased strain above 40 as shown in Fig. 4d. The extent of contact between the segments and the number of segments joined together decrease. At cutting speed of 1200 m/min, the short serrated chips with only a few segments joined together are produced. The transformed bands are already 3 μm in width, and sharp tip cracks with length of about 35 μm are generated, as shown in Fig. 4e. With cutting speed increasing up to 1300 m/min, the cracks propagate completely along the bands and tear up the chip segments into tiny debris, forming the isolated segments, as shown in Fig. 4f. Therefore, the serrated chip development in high-speed machining incubates a process of adiabatic shear evolution with the cutting speed increasing, including the formation of deformation band, transformation band, and the crack propagation in band.

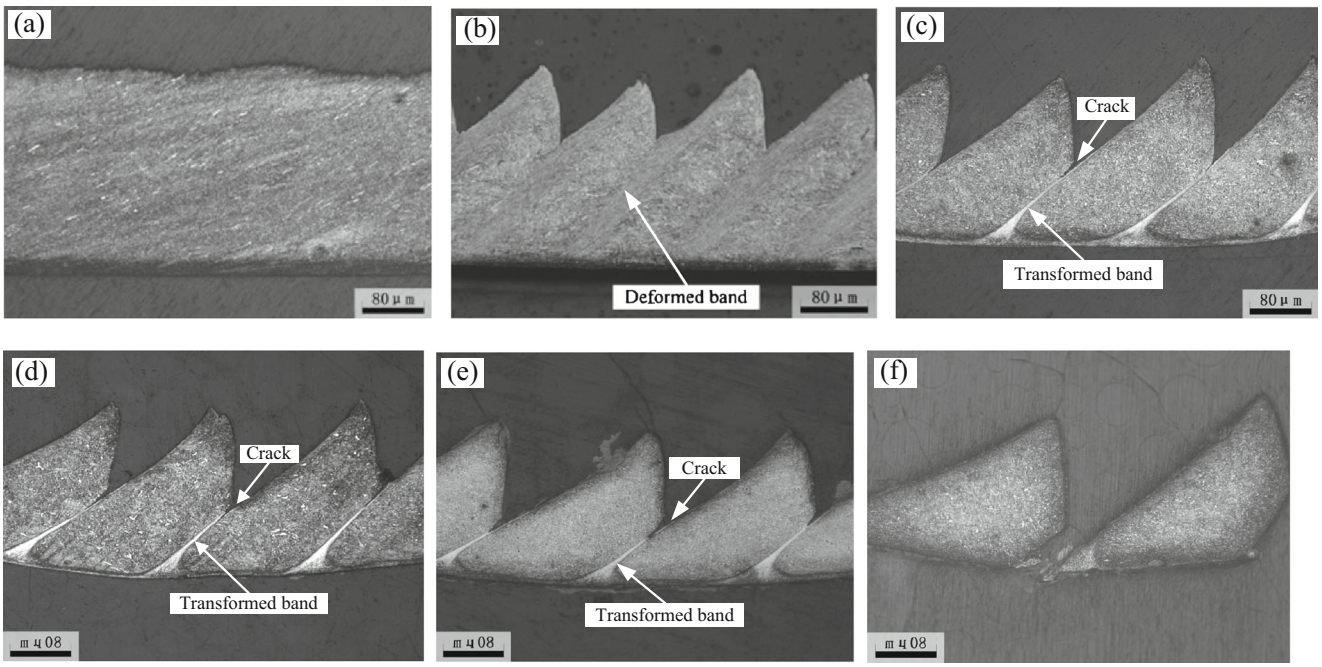

Fig. 4 The change of chip morphologies with cutting speed: **a** ribbon chip at 100 m/min; **b** deformed band at 500 m/min; **c** transformaed band at 800 m/min; **d** transformed band with crack at 1000 m/min; **e** transformed band with crack at 1200 m/min; **f** isolated segments at 1300 m/min

The experimental calculation results of strain, stress, and energy in ASB with the cutting speed are shown in Fig. 5. It is found that with the cutting speed increasing, the strain in ASB has a rapid increase up to 40 from 500 to 800 m/min due to the transition from deformed band to transformed band, and has a sharp increase up to nearly 70 from 1200 to 1300 m/min due to the transition from transformed band to fracture. And then, the strain in ASB has a slight decrease at cutting speed of 1400 m/min. Meanwhile, with the increase of cutting speed, the width of ASB decreases and the strain rate in ASB increases continuously. Thus, the stress in ASB increases sharply from 500 to 800 m/min due to the transformed band formation and then increases gradually from 800 to 1400 m/min with a decreasing growth rate up to nearly 5.5×10^8Pa. The no-growth strain in ASB after 1300 m/min may result in a moderate growth rate in temperature rise, which probably brings a decreasing growth rate in stress after the cutting speed of adiabatic shear fracture, as shown in Fig. 5. Generally, higher cutting speed leads to higher energy convergence in ASB. And, the trends of energy convergence settle to a stable limit value above 5×10^9J·m^{-2} for the decreasing growth rate in strain, stress, and temperature after the occurrence of adiabatic shear fracture. The critical cutting conditions of adiabatic shear fracture in high-speed machining of hardened steel are listed in Table 4. It can be concluded that the further increase of the cutting speed is the key condition leading to an invariability of energy in ASB when the cutting speed exceeds the critical values. Therefore, the rate-related characteristic in adiabatic shear evolution in high-speed machining is distinctly different from other high-speed impacting conditions. This fracture phenomenon is going to happen in such widely used hardened steel once the cutting speed increases large enough. Additionally, the change of chip morphology accompanies adiabatic shear evolution which contains the formation of deformed band, transformed band, crack propagation in band, and chip fracture. With the cutting speed increasing, adiabatic shear fracture takes place immediately to form tiny debris when the energy convergence in ASB reaches this saturated limit value in high-speed machining. As soon as the energy convergence in ASB exceeds this limit, the serrated chip changes into the isolated segments, which transits the cut from continuity to discontinuity. As for a single process of adiabatic shear fracture in an isolated segment formation, the deformation in ASB dose does not increase and the growth rate in stress and temperature decreases with the increase of cutting speed. Thus, the energy consumption in primary shear zone during material removal is no longer changing or keeps being a constant. It can be inferred that high-speed cutting process has a possibility in reducing the stress, temperature, and energy in ASB through utilizing the occurrence of adiabatic shear fracture and the machinability can be further optimized especially in the chip formation aspect.

Table 4 Critical cutting conditions of adiabatic shear fracture of the hardened steel

Feed: f (mm r^{-1})	0.2	0.3	0.4
Cutting speed: v (m min^{-1})	1300	900	800

4.2 Damage mechanism

The morphology of fractured shear band surface demonstrates the damage process of adiabatic shear fracture. The microscopic morphology of the fractured surface of isolated segment obtained at cutting speed of 1300 m/min is inspected by using SEM, and its viewing direction is vertical to the fractured surface, as shown in Fig. 6a. The structure distribution of the fractured surface is illustrated in Fig. 6b. The SEM micrographs of the fractured surface corresponding

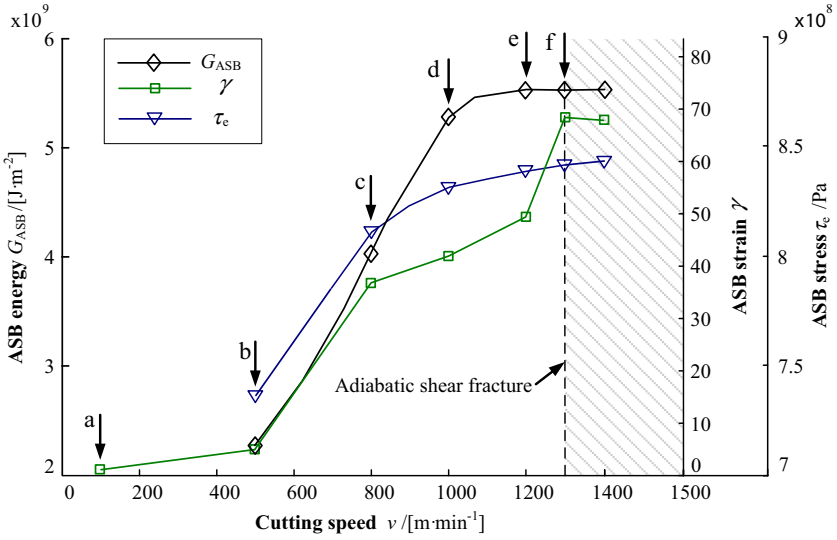

Fig. 5 Calculation results of strain, stress, and energy in ASB of different serrated chip morphologies with cutting speed

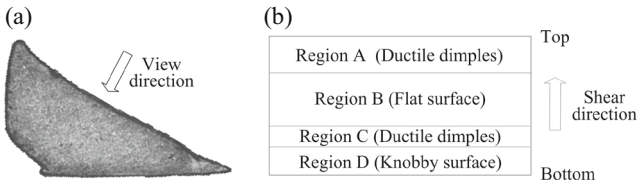

Fig. 6 **a** Micrograph of isolated segment at cutting speed of 1300 m/min; **b** microtopography distribution on the fractured surface of isolated segment

to Fig. 6b are shown in Fig. 7. It is found that there are four distinct regions formed along the shear direction. On the upside of the fractured surface (region A), elongated dimples are evident and shown in Fig. 7a. Region B is the flat surface shown in Fig. 7b. The flat surface of region B transforms into region C with elongated dimples which are larger than those on region A due to higher softening effect resulting from continuous heating near by the tool tip shown in Fig. 7c. On region D, flat surface transforms into small knobby structure shown in Fig. 7d.

The voids nucleate, grow, and coalesce, common characteristics in shear fracture process. The dimple structure means ductile fracture which is frequently observed on the cup-cone shear surfaces found on quench-hardened and tempered steels in high-velocity-impact tests at strain rates in excess of 10^3 s^{-1} [18]. The flat fracture surface implies that a sharp-tip crack forms and brittle fracture takes place in transformed band. The formation of knobby structure is similar with the high rate torsion tests [19, 20]. The severe friction between the two new fracture surfaces with bigger dimples near the tool tip leads to more heat concentration, and thus melting state in the crack tip becomes possible. It merges the dimples and the surface losing the direction, forming knobby structure due to fast cooling. Thus, for the uniformity of stress and thermal state from the tool tip to the free surface in band, it is not a single process from the onset of adiabatic shear banding to its complete fracture. The fracture mechanism of adiabatic shear fracture early exhibits ductile microvoid coalescence. And then, microcrack with sharp tip immediately initiates through the void coalescence and propagates fast along the transformed band to the chip bottom. For the influence of thermal softening effect, the damage in band transforms from brittle crack propagation to bigger ductile void coalescence, which is similar with the research of Barry et al. [10]. Finally, the downside fractured surface of transformed band is covered by knobby structure resulting from higher softening effect when shear band fractures completely. Therefore, adiabatic shear fracture in machining hardened steel is a ductile–brittle transition fracture, involving void coalescence, crack propagation, and even fusing state.

4.3 Fracture process

The process of adiabatic shear fracture is observed in the chip root morphologies which are obtained through the quick-stop tests, as shown in Fig. 8. The chip root in Fig. 8a records the onset stage of adiabatic shear in primary shear zone in which the thermal plastic localized shear region conceives and propagates to free surface. In this stage, the plastic localized shear

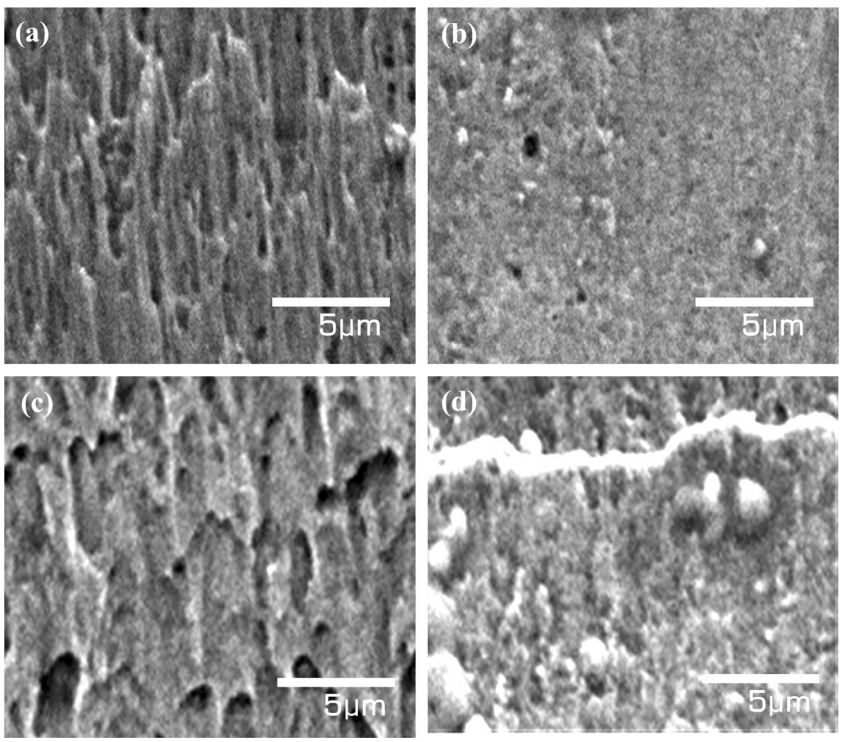

Fig. 7 Microscopic morphologies of fractured surface of isolated segments by using SEM [14]: **a** small ductile dimples; **b** flat surface; **c** big ductile dimples; **d** knobby surface

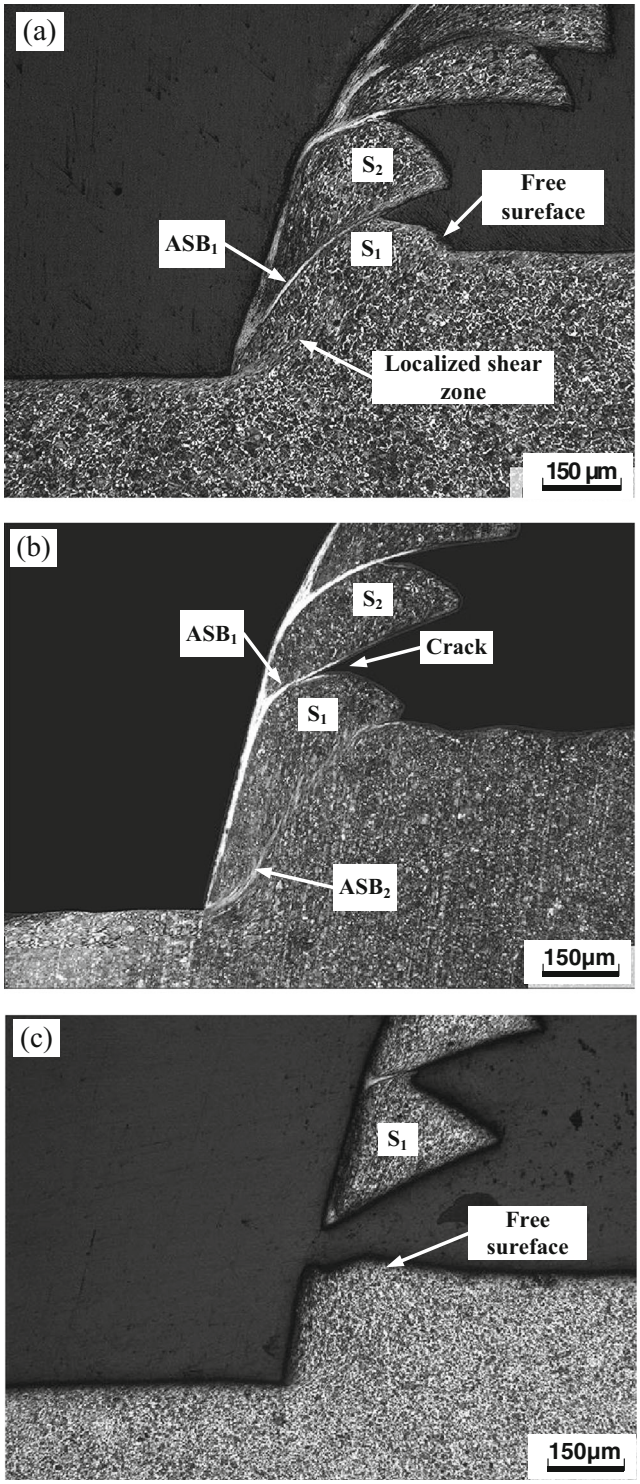

Fig. 8 The multiple process of adiabatic shear fracture is observed in the chip root morphologies obtained through quick-stop tests under high-speed machining: **a** onset of adiabatic shear; **b** formation of transformed band with crack; **c** adiabatic shear fracture

region in primary shear zone forms deformed band, and the transformed band (ASB_1) near the secondary shear zone has formed from the localized shear region. No cracks can be found on the free surface; thus, the serrated chip is formed due to the occurrence of adiabatic shear. The chip root in Fig. 8b shows that the color of deformed band turns to white and the boundary is distinct. Meanwhile, a crack in the transformed band (ASB_1) forms and propagates with the cutting tool moving forward. The chip root in Fig. 8c shows the final stage of adiabatic shear fracture. The chip segments fracture and isolate from the workpiece completely along the shear band with the segment pushed out by the cutting tool. Thus, it can be seen from these chip root morphologies that the serrated chip is formed due to the occurrence of adiabatic shear, while the isolated segments are generated due to adiabatic shear fracture.

Although the time of adiabatic shear fracture in high-speed machining is very short, the fracture process goes through the adiabatic shear evolution. The thermal softening effect takes up the leading position during the late fracture process. The strength of adiabatic shear band decreases rapidly when the crack forms in band. According to the observed results of the chip root specimens obtained from the quick-stop tests in high-speed machining, the physical model of adiabatic shear fracture in serrated chip is built up, as shown in Fig. 9. In stage I, as shown in Fig. 9a, the free surface elevates with the tool moving forward, the segment S_1 is pushed and pressed, and the localized shear region that exhibits thermo-plastic effect propagates to the whole shear plane and forms localized deformation region. The colors between deformation region and its surrounding matrix are not obviously distinct. The deformation of material in primary shear zone is constrained to localized shear region under the effect of shear force τ_1, and the energy of a small element A in band begins to concentrate. In stage II, the cutting tool goes on moving forward, and the energy of localized shear region increases until the shear band ASB_1 and chip segment S_1 form, as shown in Fig. 9b. Consequently, shear band ASB_1 bends under the pressure of the cutting tool, forming a new plastic region under the shear force τ_2, and the shear angel ϕ increases up to ϕ'. In stage III, with the cutting tool pushing the chip segment S_1 upward, the angel ϕ' keeps on increasing and the energy of element A in the shear band ASB_1 gradually concentrates to saturation limit [15], and then a propagating crack forms in the shear band ASB_1. Meanwhile, the material in chip segment S_1 repeats the stage I, localized shear region forms under the shear stress τ_3, and shear angel ϕ' goes back to ϕ. Then, the localized shear region forms shear band ASB_2 under the shear force τ_3; the energy of the element B begins to concentrate. In the stage IV, the energy in shear band ASB_2 accumulates to saturation limit, which leads to energy releasing immediately in the form of band collapse. In this stage, crack propagates completely along the shear band, which results in the segment S_1 separating from the cutting and forming isolated segments. The root of shear band ASB_2 near the chip bottom happens to bend under the extruding effect of the cutting tool, and the energy in shear band ASB_2 continues to concentrate. After

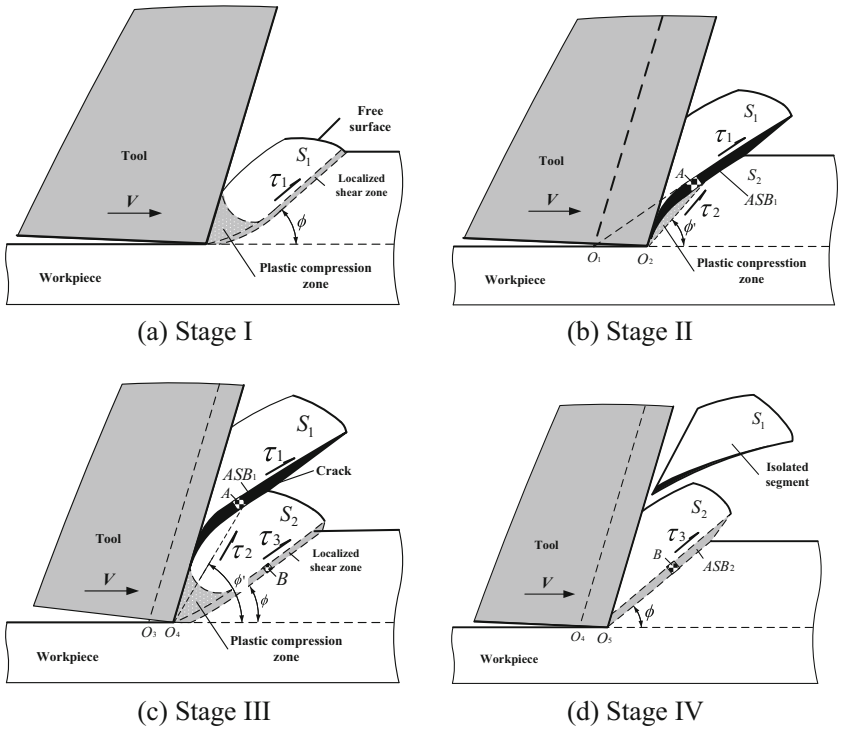

Fig. 9 Physical model of adiabatic shear fracture in isolated segment formation

this stage, the deformation of segment S_2 will repeat stage III. Therefore, the isolated segments continuously generate due to the periodic energy concentration and release. It can be inferred that the process of ASB formation and fracture are essentially the processes of energy concentration and release in the primary shear zone in high-speed machining. Once the energy convergence in ASB exceeds the saturation limit, the ASB immediately collapses to release the energy and thus form isolated segments.

5 Conclusions

1. Adiabatic shear evolution in high-speed machining of hardened steel is a process with a rate-related characteristic, including onset of adiabatic shear, deformation band, transformation band, and adiabatic shear fracture with the cutting speed increasing. Serrated chip is formed due to the occurrence of adiabatic shear, while the isolated segment is formed due to adiabatic shear fracture.
2. The damage process of adiabatic shear fracture in high-speed machining of hardened steel is a ductile–brittle transition, including void coalescence, crack propagation, and even fusing state due to the inhomogeneous thermal–mechanical distribution in band. Thermal softening effect plays a significant role on the late stage of adiabatic shear fracture.
3. The formation and fracture of ASB are the periodic processes of energy convergence and release. Once the energy convergence in ASB exceeds the saturation limit with the increase of cutting speed, the ASB immediately collapses to release the energy and thus form isolated segments.
4. It can be inferred from the experiment results that there are possibilities of reducing the increase rate of stress, temperature, and energy in ASB and optimizing the machinability especially in the chip formation aspect further through utilizing the occurrence of adiabatic shear fracture in high-speed machining. This work paves an experimental and theoretical foundation for further understanding of the high-speed machining process.

Acknowledgment This work is supported by National Natural Science Foundation of China (51175063) and assisted by Mould & Die Research Institute of Dalian University of Technology and State key Laboratory of Traction Power of Southwest Jiaotong University.

Appendix

Notation

t	Time (s)
v	Cutting velocity (m/s)
a_c	Cutting thickness (m)
a_h	Height of serrated tooth (m)
a_{ch}	Chip thickness (m)
β	Taylor and Quinney coefficient
ϕ	Nominal shear angle (degrees)
γ_0	Rake angle (degrees)

S	Shear band width (μm)
σ	Compressive stress (MPa)
τ	Shear stress (MPa)
τ_e	Equivalent shear stress (MPa)
$\tau(\gamma, \dot{\gamma}, \theta)$	Constitutive relation (MPa)
γ	Shear strain
$\dot{\gamma}$	Shear strain rate (s^{-1})
θ	Temperature (K)
θ_r	Initiate temperature (K)
θ_m	Melt temperature (K)
ρ	Mass density (kg/m^3)
c	Thermal specific capacity (J/(kg·K))
A	Modified Johnson–Cook constitutive model parameter (MPa)
B	Modified Johnson–Cook constitutive model parameter (MPa)
C	Modified Johnson–Cook constitutive model parameter
n	Modified Johnson–Cook constitutive model parameter
m_1	Modified Johnson–Cook constitutive model parameter
m_2	Modified Johnson–Cook constitutive model parameter
G_{ASB}	ASB energy (J/m^2)

References

1. Recht R (1964) Catastrophic thermoplastic shear. J Appl Mech 31: 189–193
2. Semiatin S, Rao S (1983) Shear localization during metal cutting. Mater Sci Eng 61:185–192
3. Xie J, Bayoumi A, Zbib H (1998) FEA modeling and simulation of shear localized chip formation in metal cutting. Int J Mach Tool Manuf 38:1067–1087
4. Hou Z, Komanduri R (1997) Modeling of thermomechanical shear instability in machining. Int J Mech Sci 39:1273–1275
5. Guohe L, Minjie W, Chunzheng D (2009) Adiabatic shear critical condition in the high-speed cutting. J Mater Process Technol 209: 1362–1367
6. Bai Y, Dodd B (1992) Adiabatic shear localization. Pergamon Press, Oxford
7. Wright T (2002) The physics and mathematics of adiabatic shear bands. Cambridge University Press, New York
8. Komanduri R, Schroeder T, Hazra J, Von Turkovich B, Flom D (1982) On the catastrophic shear instability in high-speed machining of an AISI 4340 steel. J Eng Ind Trans ASME 104:121–131
9. Gente A, Hoffmeister H, Evans C (2001) Chip formation in machining Ti6Al4V at extremely high cutting speeds. Cirp Ann-Manuf Technol 50:49–52
10. Barry J, Byrne G, Lennon D (2001) Observations on chip formation and acoustic emission in machining Ti6Al4V alloy. Int J Mach Tool Manuf 41:1055–1070
11. Hua J, Shivpuri R (2004) Prediction of chip morphology and segmentation during the machining of titanium alloys. J Mater Process Tech 150:124–133
12. Su G, Liu Z (2010) An experimental study on influences of material brittleness on chip morphology. Int J Adv Manuf Technol 51:87–92
13. Minjie W, Chunzheng D, Hongbo L (2004) Experimental Study on Adiabatic Shear Behavior in Chip Formation during Orthogonal Cutting. Chin J Mech Eng 7–10
14. Liyao G, Minjie W, Chunzheng D (2013) On adiabatic shear localized fracture during serrated chip evolution in high speed machining of hardened AISI 1045 steel. Int J Mech Sci 75: 288–298
15. Liyao G, Minjie W (2013) Experimental and theoretical research on critical characteristics for adiabatic shear localization fracture in high-speed machining. Int J Adv Manuf Technol 68:1231–1240
16. Feng Z, Li G, Meng D (2010) A study on material dynamic plastic constitutive relationship considering hardness. Mech Autom Control Eng (MACE), 2010 Int Conf IEEE 3686–3689
17. Buda J (1972) New methods in the study of plastic deformation in cutting zone. Annals CIRP 21:17–18
18. Odeshi A, Bassim M (2009) High strain-rate fracture and failure of a high strength low alloy steel in compression. Mater Sci Eng A 525:96–101
19. Giovanola J (1988) Adiabatic shear banding under pure shear loading part II: fractographic and metallographic observations. Mech Mater 7:73–87
20. Rogers H (1983) Adiabatic shearing—general nature and material aspects, Material behavior under high stress and ultrahigh loading rates. Plenum Press, New York, pp 101–118